γ-ray strength function for barium isotopes

H. Utsunomiya,[1,*] T. Renstrøm,[2] G. M. Tveten,[2] S. Goriely,[3] T. Ari-izumi,[1] V. W. Ingeberg,[2] B. V. Kheswa,[2,4] Y.-W. Lui,[5] S. Miyamoto,[6] S. Hilaire,[7] S. Péru,[7] and A. J. Koning[8]

[1]*Konan University, Department of Physics, 8-9-1 Okamoto, Higashinada, Kobe 658-8501, Japan*

[2]*Department of Physics, University of Oslo, N-0316 Oslo, Norway*

[3]*Institut d'Astronomie et d'Astrophysique, Université Libre de Bruxelles, Campus de la Plaine, CP-226, 1050 Brussels, Belgium*

[4]*Department of Applied Physics and Engineering Mathematics, University of Johannesburg, Doornfontein, Johannesburg 2028, South Africa*

[5]*Cyclotron Institute, Texas A& M University, College Station, Texas 77843, USA*

[6]*Laboratory of Advanced Science and Technology for Industry, University of Hyogo, 3-1-2 Kouto, Kamigori, Ako-gun, Hyogo 678-1205, Japan*

[7]*CEA, DAM, DIF, F-91297 Arpajon, France*

[8]*Nuclear Data Section, International Atomic Energy Agency, A-1400 Vienna, Austria*

(Received 18 June 2019; published 4 September 2019)

Photoneutron cross sections were measured for ^{137}Ba and ^{138}Ba at energies below two-neutron threshold using quasimonochromatic γ-ray beams produced in laser Compton scattering at the NewSUBARU synchrotron radiation facility. The photoneutron data are used to constrain the γ-ray strength function on the basis of the Hartree-Fock-Bogolyubov plus quasiparticle random phase approximation using the Gogny $D1M$ interaction. Supplementing the experimentally constrained γ-ray strength function with the zero-limit $E1$ and $M1$ contributions, which are unique to the deexcitation mode, we discuss radiative neutron capture cross sections relevant to the s-process nucleosynthesis of barium isotopes in the vicinity of the neutron magic number 82.

DOI: 10.1103/PhysRevC.100.034605

I. INTRODUCTION

The γ-ray strength function (γSF) [1,2] is a statistical quantity employed in the Hauser-Feshbach model of the compound nuclear reaction. The γSF in the deexcitation mode is a key quantity to determine radiative neutron capture cross sections that are of direct relevance to the s-process nucleosynthesis of elements heavier than iron. The downward γSF for dipole radiation with a given energy ε_γ is defined [3] by

$$\overleftarrow{f_{X1}}(\varepsilon_\gamma) = \varepsilon_\gamma^{-3}\frac{\langle\Gamma_{X1}(\varepsilon_\gamma)\rangle}{D_\ell}. \quad (1)$$

Here X is either electric (E) or magnetic (M), $\langle\Gamma_{X1}(\varepsilon_\gamma)\rangle$ is the average radiation width, and D_ℓ is the average level spacing for s-wave ($\ell = 0$) or p-wave ($\ell = 1$) neutron resonances.

In contrast, the γSF in the excitation mode for dipole radiation is defined [3] by the average cross section for $E1/M1$ photoabsorption $\langle\sigma_{X1}(\varepsilon_\gamma)\rangle$ to the final states with all possible spins and parities [2]:

$$\overrightarrow{f_{X1}}(\varepsilon_\gamma) = \frac{\varepsilon_\gamma^{-1}}{3(\pi\hbar c)^2}\langle\sigma_{X1}(\varepsilon_\gamma)\rangle. \quad (2)$$

Above neutron separation energy except at energies near neutron threshold, the total upward γSF can be determined by substituting $\langle\sigma_{X1}(\varepsilon_\gamma)\rangle$ with experimental photoneutron cross sections that dominate photoabsorption cross sections.

A recent systematic study across the chart of nuclei has formulated the zero-limit behavior of both $E1$ and $M1$ strengths in the analytical form [4], the latter of which (referred to as $M1$ up-bend) was experimentally observed [5–7] and theoretically supported by the shell-model calculation [8–13]. The presence of the zero-limit strengths, which correspond to γ-ray transitions between high-lying states is unique to the downward γSF, showing that the Brink hypothesis of the approximate equality of $\overleftarrow{f_{X1}}$ and $\overrightarrow{f_{X1}}$ [14,15] is violated.

The radiative neutron capture in the s-process path, which proceeds along the valley of β stability successively produce heavier isotopes by adding one neutron at a time until it is intervened by β^- decay, which increases the atomic number of the element by one. When the s-process flow reaches a magic neutron number, the nuclear binding energy increases by an amount of the order of 1–2 MeV, leading to a drop of the neutron separation energy of a compound nucleus, which is formed by the neutron capture. The drop results in large level spacing D in Eq. (1), and significantly decreases the downward γSF and radiative neutron capture cross section of neutron magic nuclei [16]. As a result, the s-process nucleosynthesis forms the first, second, and third peaks of elements around the mass number A = 86–90, 138–142, and 208, corresponding to the magic number 50, 82, and 126, respectively.

In this paper, we discuss radiative neutron capture cross sections for barium isotopes including ^{138}Ba with the neutron magic number 82 in terms of the deexcitation γSF based on the γ-ray strength function method [17,18]. The γSF from two relatively different nuclear models are studied, namely

*hiro@konan-u.ac.jp

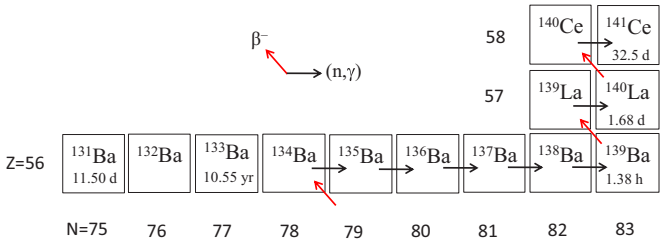

FIG. 1. An excerpt of the chart of nuclei depicting the Ba region along the *s*-process path.

the simple modified Lorentzian (SMLO) model [19] and the Hartree-Fock-Bogolyubov plus quasiparticle random phase approximation (QRPA) based on the Gogny $D1M$ interaction (hereafter denoted as $D1M$ + QRPA) [4,20,21] for both $E1$ and $M1$ components is constrained to the present photoneutron cross section measured for ^{138}Ba and, for the first time, ^{137}Ba. The experimentally constrained γSF is further supplemented with the zero-limit $E1$ and $M1$ contributions, which are unique to the deexcitation mode.

Based on the same nuclear ingredients, radiative neutron capture cross sections are calculated with the TALYS code [22] for other stable barium isotopes including ^{138}Ba and compared with experimental data. The Ba isotopes of the present research interest along the *s*-process path are shown in Fig. 1.

In Sec. II, our experimental procedure is described and in Sec. III data are analyzed. Our resulting photoneutron cross sections are discussed in Sec. IV and compared with $D1M$ + QRPA calculations. Radiative neutron capture cross sections calculated for stable barium isotopes are compared with experimental data. Finally, conclusions are drawn in Sec. V.

II. EXPERIMENTAL PROCEDURE

The photoneutron measurements on ^{137,138}Ba took place at the NewSUBARU synchrotronic radiation facility. Quasimonochromatic pencil-like γ-ray beams were produced through laser Compton scattering (LCS) of 1064 nm photons from the Nd:YVO_4 laser in head-on collisions with relativistic electrons. The electrons were injected from a linear accelerator into the NewSUBARU storage ring with an initial energy of 974 MeV, then subsequently decelerated to nominal energies in the region from 620 and 694 MeV to 849 MeV, providing LCS γ-ray beams corresponding to the neutron separation energy S_n up to 13 MeV for ^{137}Ba and ^{138}Ba, respectively. In total, 22 and 15 individual γ beams were produced for both ^{137}Ba and ^{138}Ba, respectively.

The ^{137,138}Ba targets were made form isotopically enriched barium carbonate ($BaCO_3$). The material was in pressed together and enclosed in an Al cylinder with a thin cap. The targets had areal density of 2.236 g/cm^2 and 5.642 g/cm^2, for ^{137}Ba and ^{138}Ba, respectively. The presence of the Al cap made it necessary not to increase the γ-ray beam energy above 13 MeV due to S_n = 13.056 MeV for ^{27}Al. The corresponding enrichment of the two isotopes were 85.0% and 99.9%. The main contaminant of the ^{137}Ba target was ^{138}Ba (≈15%). This

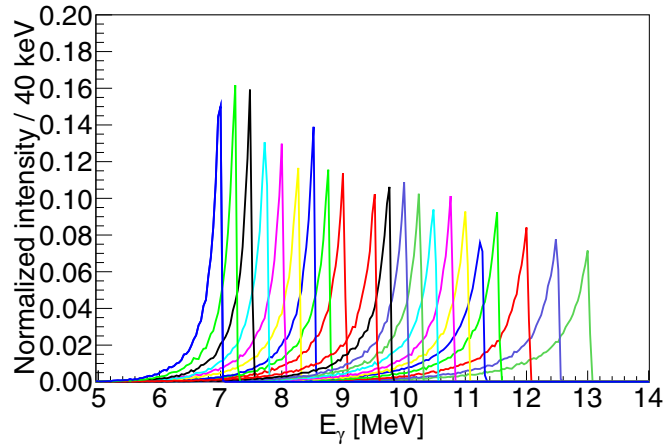

FIG. 2. The simulated energy profiles for the γ beams used in the ^{137,138}Ba measurements. The distributions are normalized to unity.

was taken into account by using only the number of ^{137}Ba nuclei below S_n of ^{138}Ba, 8611.72 keV, and by considering the neutron contribution from ^{138}Ba above.

The LCS γ-ray beam produced at NewSUBARU is well calibrated in absolute energy [23], energy profile [24–26], and flux [27,28]. One can find more details of generation and calibration of the LCS γ-ray beam, and detection of neutrons with a high-efficiency moderation-based detector [29] in Ref. [18].

The measured photoneutron cross section for an incoming beam with maximum γ energy $E_{\max}$ is given by the convoluted cross section,

$$\sigma_{\rm exp}^{E_{\max}} = \int_{S_n}^{E_{\max}} D^{E_{\max}}(E_\gamma)\sigma(E_\gamma)dE_\gamma = \frac{N_n}{N_t N_\gamma \xi \epsilon_n g}. \quad (3)$$

Here, $D^{E_{\max}}$ is the normalized, $\int_{S_n}^{E_{\max}} D^{E_{\max}} dE_\gamma = 1$, energy distribution of the γ-ray beam obtained from a GEANT4 [30] simulation analysis of experimental response functions of a $LaBr_3$(Ce) beam-profile monitor. The simulated profiles of the γ beams, $D^{E_{\max}}$, used to investigate ^{137}Ba are shown in Fig. 2. Furthermore, $\sigma(E_\gamma)$ is the true photoneutron cross section as a function of energy. The quantity N_n represents the number of neutrons detected, N_t gives the number of target nuclei per unit area, N_γ is the number of γ rays incident on target, ϵ_n represents the neutron detection efficiency, and finally $\xi = (1 - e^{-\mu t})/(\mu t)$ gives a correction factor for self-attenuation in the target. The factor g represents the fraction of the γ flux above S_n.

We have determined the convoluted cross sections $\sigma_{\rm exp}^{E_{\max}}$ given by Eq. (3) for γ beams with maximum energies in the range $S_n \leqslant E_{\max} \leqslant 13$ MeV. The convoluted cross sections $\sigma_{\rm exp}^{E_{\max}}$ are not connected to a specific E_γ, and we choose to plot them as a function of $E_{\gamma\max}$. The convoluted cross sections of the two Ba isotopes, which are often called monochromatic cross sections, are shown in Fig. 3. The error bars in Fig. 3 represent the total uncertainty in the quantities comprising Eq. (3) and consists of ≈3.2% from the efficiency of the neutron detector, ≈1% from the pileup method that gives the number of γ rays, and the statistical uncertainty in the number

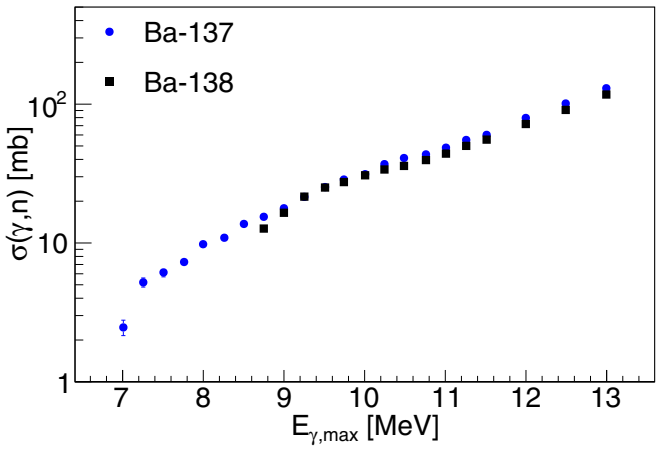

FIG. 3. Monochromatic cross sections of ^{137}Ba and ^{138}Ba. The error bars contain statistical uncertainties from the number of detected neutrons, the uncertainty in the efficiency of the neutron detector and the uncertainly in the pileup method used to determine the number of incoming γ's on target.

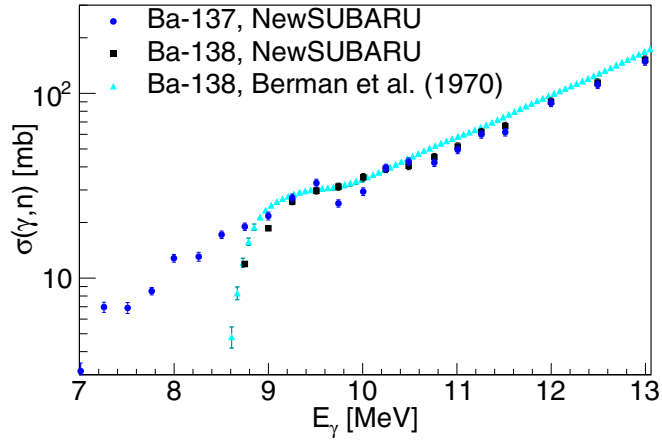

FIG. 4. Unfolded cross sections of ^{137,138}Ba in comparison with the previous measurements for ^{138}Ba [34].

of detected neutrons. The statistical error ranges between ≈13% close to neutron threshold and 4.6% for the highest maximum γ-ray beam energies. Except for the first few data points close to separation energy, the total error is dominated by the uncertainty stemming from the pileup method and from the simulated efficiency of the neutron detector. For the total uncertainty, we have added these uncorrelated errors quadratically.

III. DATA ANALYSIS

Now we extract the deconvoluted, E_γ dependent, photoneutron cross section, $\sigma(E_\gamma)$, from the integral of Eq. (3) [31]. Each of the measurements characterized by the beam energy, $E_{\max}$, corresponds to folding of $\sigma(E_\gamma)$ with the measured beam profile, $D^{E_{\max}}$. By approximating the integral in Eq. (3) with a sum for each γ-beam profile, we are able to express the problem as a set of linear equations

$$\sigma_{\mathrm{f}} = \mathbf{D}\sigma, \tag{4}$$

where σ_{f} is the cross section folded with the beam profile $\mathbf{D}$. The indexes i and j of the matrix element $D_{i,j}$ corresponds to $E_{\max}$ and E_γ, respectively. The set of equations is given by

$$\begin{pmatrix} \sigma_1 \\ \sigma_2 \\ \vdots \\ \sigma_N \end{pmatrix}_{\mathrm{f}} = \begin{pmatrix} D_{11} & D_{12} & \cdots & \cdots & D_{1M} \\ D_{21} & D_{22} & \cdots & \cdots & D_{2M} \\ \vdots & \vdots & \vdots & \vdots & \vdots \\ D_{N1} & D_{N2} & \cdots & \cdots & D_{NM} \end{pmatrix} \begin{pmatrix} \sigma_1 \\ \sigma_2 \\ \vdots \\ \vdots \\ \sigma_M \end{pmatrix}. \tag{5}$$

Each row of $\mathbf{D}$ corresponds to a GEANT4 simulated γ-beam profile belonging to a specific measurement characterized by $E_{\max}$. See Fig. 2 for a visual representation of the response matrix $\mathbf{D}$. It is clear that $\mathbf{D}$ is highly asymmetrical.

As mentioned, we have used $N = 15$ beam energies when investigating ^{137}Ba and 18 for ^{138}Ba, but the beam profiles above S_n is simulated in steps of 10 keV in γ-ray energy. As the system of linear equations in Eq. (5) is underdetermined, the true σ vector cannot be extracted by matrix inversion. In order to find σ, we utilize a folding iteration method. The main features of this method are as follows:

(i) As a starting point, we choose for the zeroth iteration, a constant trial function σ^0. This initial vector is multiplied with $\mathbf{D}$, and we get the zeroth folded vector $\sigma_{\mathrm{f}}^0 = \mathbf{D}\sigma^0$.

(ii) The next trial input function, σ^1, can be established by adding the difference of the experimentally measured spectrum, σ_{exp}, and the folded spectrum, σ_{f}^0, to σ^0. In order to be able to add the folded and the input vector together, we first perform a piecewise cubic Hermite interpolating polynomial (pchip) interpolation on the folded vector so that the two vectors have equal dimensions. Our new input vector is

$$\sigma^1 = \sigma^0 + \left(\sigma_{\mathrm{exp}} - \sigma_{\mathrm{f}}^0\right). \tag{6}$$

(iii) The steps (i) and (ii) are iterated i times giving

$$\sigma_{\mathrm{f}}^i = \mathbf{D}\sigma^i \tag{7}$$

$$\sigma^{i+1} = \sigma^i + \left(\sigma_{\mathrm{exp}} - \sigma_{\mathrm{f}}^i\right) \tag{8}$$

until convergence is achieved. This means that $\sigma_{\mathrm{f}}^{i+1} \approx \sigma_{\mathrm{exp}}$ within the statistical errors. In order to quantitatively check convergence, we calculate the reduced χ^2 of $\sigma_{\mathrm{f}}^{i+1}$ and σ_{exp} after each iteration. Approximately four iterations are usually enough for convergence, which is defined when the reduced χ^2 value approaches ≈1.

We stopped iterating when the χ^2 started to be lower than unity. In principle, the iteration could continue until the reduced χ^2 approaches zero, but that results in large unrealistic fluctuations in σ^i due to overfitting to the measured points σ_{exp}.

We estimate the total uncertainty in the unfolded cross sections by calculating an upper limit of the monochromatic cross sections from Fig. 3 by adding and subtracting the errors to the measured cross-section values. This upper and lower limit is then unfolded separately, resulting in the unfolded cross sections shown in Fig. 4.

TABLE I. The unfolded cross sections σ evaluated at the maximum γ-ray energy and the total (statistical plus systematic) uncertainty $\Delta\sigma$.

^{137}Ba	E_γ [MeV]	σ [mb]	$\Delta\sigma$ [mb]
	7.01	3.14	0.33
	7.26	6.97	0.44
	7.51	6.90	0.47
	7.76	8.51	0.40
	8.00	12.81	0.62
	8.26	13.07	0.72
	8.50	17.18	0.80
	8.75	18.99	0.87
	9.00	21,71	1.08
	9.25	27.22	1.30
	9.51	32.71	1.60
	9.74	25.38	1.16
	10.01	29.40	1.40
	10.25	39.46	1.89
	10.49	42.70	2.06
	10.76	42.14	1.95
	11.01	49.51	2.37
	11.26	59.97	2.79
	11.51	61.64	2.88
	12.00	88.85	4.11
	12.49	111.26	5.10
	13.00	148.72	6.84
^{138}Ba	E_γ [MeV]	σ [mb]	$\Delta\sigma$ [mb]
	8.75	11.93	0.27
	9.00	18.62	0.62
	9.25	25.97	1.00
	9.51	29.72	1.21
	9.74	31.28	1.39
	10.01	35.16	1.63
	10.25	39.08	1.82
	10.49	40.57	1.90
	10.76	45.16	2.15
	11.01	51.48	2.47
	11.26	61.69	2.93
	11.51	66.46	3.20
	12.00	90.04	4.35
	12.49	114.18	5.52
	13.00	151.95	7.36

In Fig. 4, the unfolded cross sections for ^{137}Ba and ^{138}Ba are evaluated at the maximum energies of the incoming γ beams. The error bars represent the difference between the upper and lower limit of the unfolded cross sections. The unfolded cross sections are tabulated in Table I.

IV. DISCUSSION

The present experimental results are now analyzed in light of the recent systematics of the γSF obtained within the phenomenological Lorentzian approach with the SMLO model [19] and within the mean field plus QRPA calculations with the $D1M$ + QRPA model [4,20,21]. While the SMLO $E1$ strength is essentially fitted on available photoabsorption data, the $D1M$ + QRPA has only globally be renormalized to

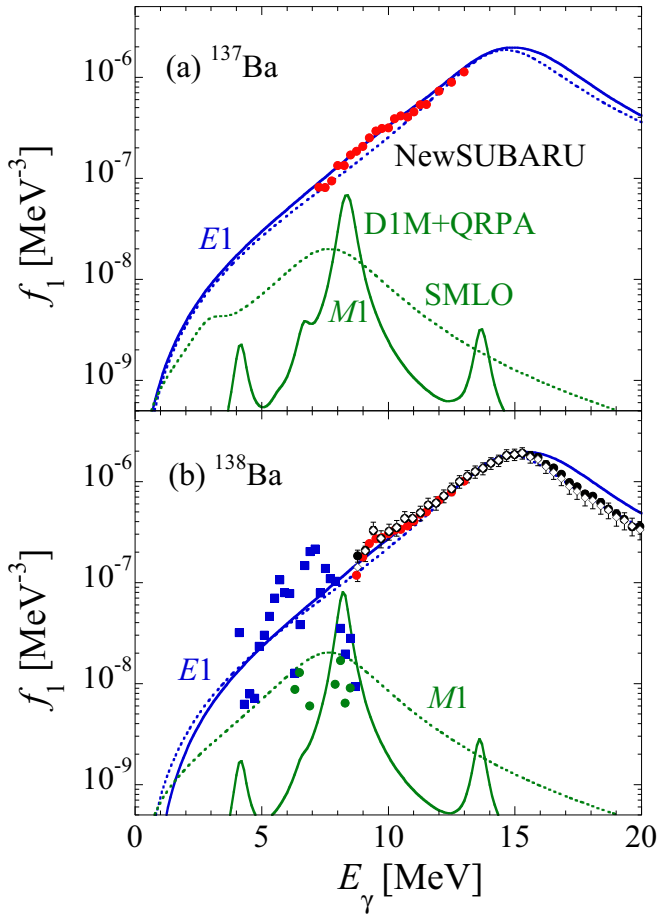

FIG. 5. (a) Comparison of the $D1M$ + QRPA (solid lines) and SMLO (dotted lines) γSF for ^{137}Ba with the measured strength function extracted from the present NewSUBARU experiment (red circles). The $E1$ mode is shown by blue lines and $M1$ by green lines. (b) same for and ^{138}Ba γSF. Previous measurements from nuclear resonance fluorescence [32] for the $E1$ (blue squares) and $M1$ (green circles) modes, as well as photoneutron data (solid circles) [34] and its evaluation (open diamonds) [35] are also shown.

reproduce the bulk of experimental data. Such a renormalization includes a broadening of the QRPA strength to take the neglected damping of collective motions into account as well as a shift of the strength to lower energies due to the contribution beyond the one-particle–one-hole excitations and the interaction between the single-particle and low-lying collective phonon degrees of freedom. Such phenomenological corrections have been applied to the present Ba isotopes, as described in Ref. [4]. In addition, in order to reproduce the present photoneutron cross section in the low-energy tail of the giant dipole resonance, we find that a global energy shift of 0.5 MeV of the overall $E1$ strength is required in the specific case of ^{138}Ba. Such renormalizations are within the uncertainties affecting the γSF predictions [4]. The resulting $D1M$ + QRPA and SMLO γSF for ^{137}Ba and ^{138}Ba are shown in Fig. 5 and compare with the present and previous data. In the case of ^{138}Ba, nuclear resonance fluorescence measurements [32] are also available separately for the $E1$ and $M1$

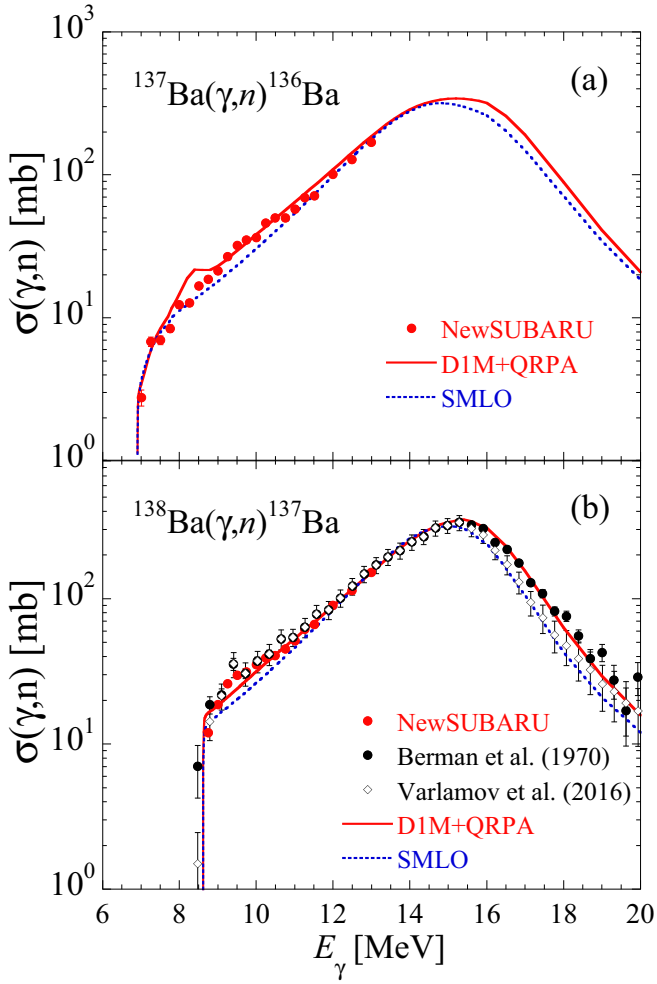

FIG. 6. (a) Present ^{137}Ba$(\gamma, n)^{136}$Ba measured cross sections compared with the TALYS calculations based on the SMLO (dashed blue line) and $D1M + \text{QRPA}$ (solid red line) γSF. (b) same for ^{138}Ba$(\gamma, n)^{137}$Ba reaction where previous measurements (black circles) [34] and evaluation (open diamonds) [35] are also shown.

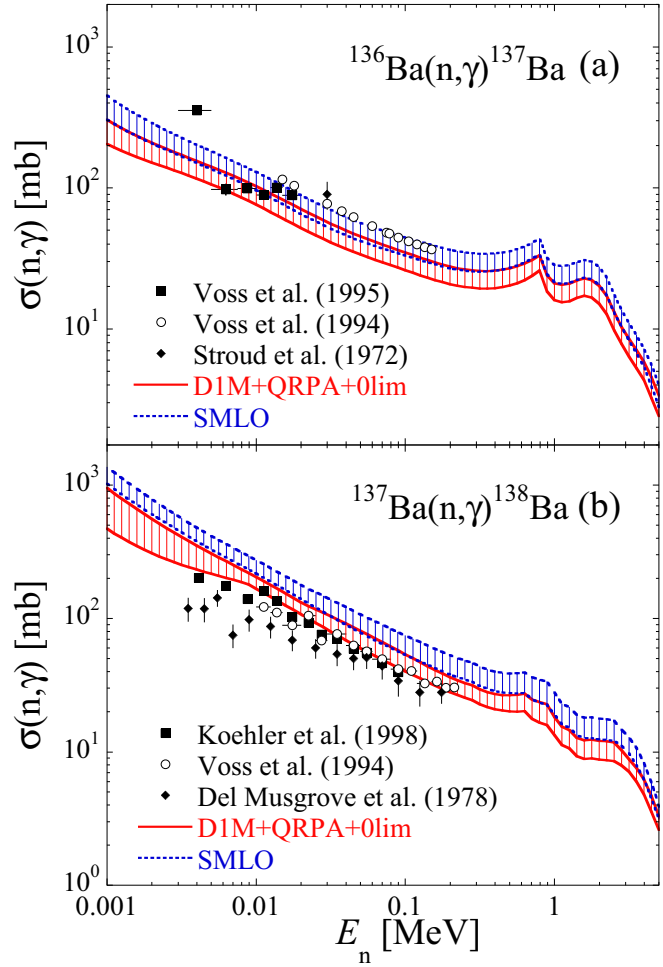

FIG. 7. (a) Comparison of the ^{136}Ba$(n, \gamma)^{137}$Ba measured cross sections [38–40] with the TALYS calculations based on the SMLO (dashed blue line) and $D1M + \text{QRPA} + 0\text{lim}$ (solid red line) γSF. (b) same for ^{137}Ba$(n, \gamma)^{138}$Ba cross section [40–42]. Theoretical uncertainties correspond to the use of different level density models [36,37].

modes. Details on the extraction of the γSF from measured data can be found in Ref. [33].

Both the $D1M + \text{QRPA}$ and SMLO models have proven their capacity to reproduce relatively well all types of experimental data bearing relevant information on γSF, such as those extracted from photoabsorption, nuclear resonance fluorescence, Oslo method, radiative neutron or proton captures, or inelastic proton experiments as shown in Ref. [33]. We show in Figs. 5 and 6 that this is also the case for the present Ba photoneutron data in the whole energy range covered by our experiment. In the ^{137}Ba$(\gamma, n)^{136}$Ba case, the $D1M + \text{QRPA}$ $M1$ spin-flip strength at 8.5 MeV is, however, clearly overestimated, while the SMLO model underestimates the $E1$ strength in the 9–11 MeV region.

Another way of testing our photoneutron data and the γSF deduced out of those is to consider the reverse radiative neutron capture cross sections. Those are available for ^{136}Ba and ^{137}Ba and therefore are sensitive to the low-energy γSF of ^{137}Ba and ^{138}Ba, respectively. We have considered both the SMLO and $D1M + \text{QRPA}$ $E1$ and $M1$ strengths as described above and applied them to the TALYS calculation of the (n, γ) cross section. It should, however, be stressed that the photoabsorption strength needs to be complemented by the zero-limit correction when considering the deexcitation of the compound nucleus formed by the neutron capture. Inspired from shell-model studies, this low-energy limit has been approximated in Ref. [4] for $D1M + \text{QRPA}$ (the model is then referred to as $D1M + \text{QRPA} + 0\text{lim}$) and in Ref. [19] for SMLO. The radiative cross sections are also sensitive to the adopted nuclear level density model. For these reasons, different prescriptions [36,37] have been considered in the TALYS calculations.

We compare in Fig. 7 the ^{136}Ba$(n, \gamma)^{137}$Ba and ^{137}Ba$(n, \gamma)^{138}$Ba measured cross sections with the TALYS Hauser-Feshbach calculation based on the $D1M + \text{QRPA} + 0\text{lim}$ and SMLO γSF and different nuclear level density prescriptions. All nuclear level densities [36,37] are normalized to the existing s-wave spacing data at the neutron binding

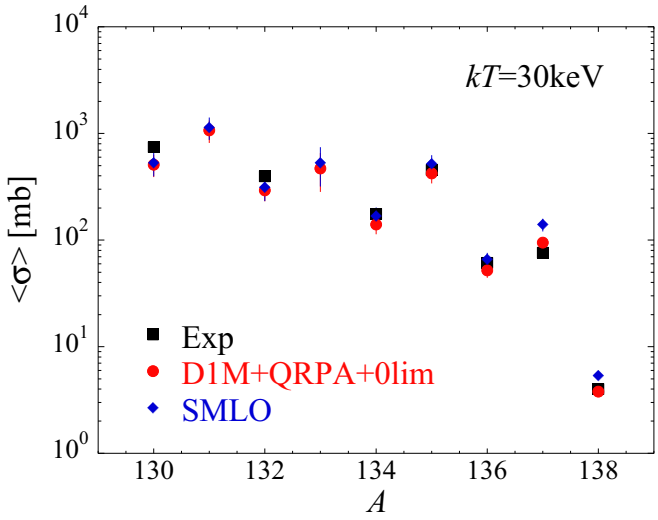

FIG. 8. Comparison between experimental (black squares) [43] and theoretical Maxwellian-averaged cross sections at 30 keV predicted by the TALYS code with $D1M$ + QRPA + 0lim (red circles) or SMLO (blue diamonds) γSF for the radiative neutron capture on Ba isotopes with A lying between 130 and 138.

energy [3]. As shown in Fig. 7, the calculated cross sections are in rather good agreement with available experimental data in the keV region, although $D1M$ + QRPA + 0lim tend to underestimate the ^{136}Ba$(n,\gamma)^{137}$Ba cross section and SMLO to overestimate the ^{137}Ba$(n,\gamma)^{138}$Ba cross section.

To further compare the predictive power of the $D1M$ + QRPA + 0lim and SMLO models, we compare in Fig. 8 the 30 keV experimental Maxwellian-averaged cross sections [43] with the TALYS predictions based again on both γSF models and different prescriptions for the nuclear level densities [36,37]. For the seven stable isotopes of Ba for which experimental values exist, the agreement is relatively good, $D1M$ + QRPA + 0lim model giving a root-mean-square deviation on the cross section ratio of 1.26 and SMLO of 1.36. The experimentally unknown Maxwellian-averaged cross sections for ^{131}Ba and ^{133}Ba can therefore be estimated within a typical uncertainty of 30%. We find for ^{131}Ba a 30 keV Maxwellian-averaged cross section of 1100 ± 300 mb and for ^{133}Ba of 500 ± 200 mb

V. CONCLUSION

We presented a new experimental determination of the (γ, n) cross section for ^{137}Ba and ^{138}Ba performed at the NewSUBARU synchrotron radiation facility. Our new measurements cover the low-energy tail of the giant dipole resonance above the neutron threshold and are found for the ^{138}Ba case to be in excellent agreement with previous measurements. In the ^{137}Ba case, photoneutron cross sections were measured for the first time in this experiment. The new cross sections were used to constrain the $E1$ and $M1$ strength functions obtained within the semimicroscopic $D1M$ + QRPA and phenomenological SMLO approaches. We have further confirmed the relevance of the experimentally constrained $D1M$ + QRPA dipole γ-ray strength function by analyzing the radiative neutron capture cross sections for Ba isotopes considering in addition the zero-limit systematics for both the deexcitation $E1$ and $M1$ strengths. Finally, the present analysis was used to estimate the Maxwellian-averaged ^{131}Ba$(n,\gamma)^{132}$Ba and ^{133}Ba$(n,\gamma)^{134}$Ba cross sections.

ACKNOWLEDGMENTS

The authors are grateful to H. Ohgaki of the Institute of Advanced Energy, Kyoto University for making a large volume $LaBr_3$(Ce) detector available for the experiment. H.U. acknowledges the support from the Premier Project of the Konan University. S.G. acknowledges the support from the F.R.S.-FNRS. G.M.T. acknowledges funding from the Research Council of Norway, Project Grant No. 262952. This work was supported by the IAEA and performed within the IAEA CRP on "Updating the Photonuclear data Library and generating a Reference Database for Photon Strength Functions" (F41032).

[1] G. A. Bartholomew, E. D. Earle, A. J. Fergusson, J. W. Knowles, and M. A. Lone, Adv. Nucl. Phys. **7**, 229 (1973).
[2] M. A. Lone, in *Neutron Induced Reactions, Proceedings of the 4th International Symposium Smolenice, Czechoslovakia*, 1985, edited by J. Kristiak and E. Betak (Springer, Dordrecht, Holland, 1986), pp. 238–252.
[3] R. Capote, M. Herman, P. Obložinský, P. G. Young, S. Goriely, T. Belgya, A. V. Ignatyuk, A. J. Koning, S. Hilaire, V. A. Plujko, M. Avrigeanu, O. Bersillon, M. B. Chadwick, T. Fukahori, Zhigang Ge, Yinlu Han, S. Kailas, J. Kopecky, V. M. Maslov, G. Reffo, M. Sin, E. Sh. Soukhovistskii, and P. Talou, Nucl. Data Sheets **110**, 3107 (2009).
[4] S. Goriely, S. Hilaire, S. Péru, and K. Sieja, Phys. Rev. C **98**, 014327 (2018).
[5] A. Voinov, E. Algin, U. Agvaanluvsan, T. Belgya, R. Chankova, M. Guttormsen, G. E. Mitchell, J. Rekstad, A. Schiller, and S. Siem, Phys. Rev. Lett. **93**, 142504 (2004).
[6] M. Guttormsen, R. Chankova, U. Agvaanluvsan, E. Algin, L. A. Bernstein, F. Ingebretsen, T. Lönnroth, S. Messelt, G. E. Mitchell, J. Rekstad, A. Schiller, S. Siem, A. C. Sunde, A. Voinov, and S. Ødegård, Phys. Rev. C **71**, 044307 (2005).
[7] E. Algin, U. Agvaanluvsan, M. Guttormsen, A. C. Larsen, G. E. Mitchell, J. Rekstad, A. Schiller, S. Siem, and A. Voinov, Phys. Rev. C **78**, 054321 (2008).
[8] R. Schwengner, S. Frauendorf, and A. C. Larsen, Phys. Rev. Lett. **111**, 232504 (2013).
[9] B. A. Brown and A. C. Larsen, Phys. Rev. Lett. **113**, 252502 (2014).
[10] K. Sieja, Phys. Rev. Lett. **119**, 052502 (2017).
[11] K. Sieja, Europhys. J. Web Conf. **146**, 05004 (2017).
[12] S. Karampagia, B. A. Brown, and V. Zelevinsky, Phys. Rev. C **95**, 024322 (2017).
[13] R. Schwengner, S. Frauendorf, and B. A. Brown, Phys. Rev. Lett. **118**, 092502 (2017).

[14] D. M. Brink, Ph.D. thesis, Oxford University, 1955.
[15] P. Axel, Phys. Rev. **126**, 671 (1962).
[16] J. M. Blatt and V. E. Weisskopf, *Theoretical Nuclear Physics*, (Springer-Verlag, New York, 1979), p. 761.
[17] H. Utsunomiya, T. Renstrøm, G. M. Tveten, S. Goriely, S. Katayama, T. Ari-izumi, D. Takenaka, D. Symochko, B. V. Kheswa, V. W. Ingeberg *et al.*, Phys. Rev. C **98**, 054619 (2018).
[18] H. Utsunomiya, T. Renstrøm, G. M. Tveten, S. Goriely, T. Ari-izumi, D. Filipescu, J. Kaur, Y.-W. Lui, W. Luo, S. Miyamoto *et al.*, Phys. Rev. C **99**, 024609 (2019).
[19] S. Goriely and V. Plujko, Phys. Rev. C **99**, 014303 (2019).
[20] M. Martini, S. Péru, S. Hilaire, S. Goriely, and F. Lechaftois, Phys. Rev. C **94**, 014304 (2016).
[21] S. Goriely, S. Hilaire, S. Péru, M. Martini, I. Deloncle, and F. Lechaftois, Phys. Rev. C **94**, 044306 (2016).
[22] A. J. Koning and D. Rochman, Nucl. Data Sheets **113**, 2841 (2012).
[23] H. Utsunomiya, T. Shima, K. Takahisa, D. M. Filipescu, O. Tesileanu, I. Gheorghe, H.-T. Nyhus, T. Renstrøm, Y.-W. Lui, Y. Kitagawa, S. Amano, and S. Miyamoto, IEEE Trans. Nucl. Sci. **61**, 1252 (2014).
[24] A. I. Gheorghe, Ph.D. thesis, University of Bucharest, 2017.
[25] D. M. Filipescu, I. Gheorghe, H. Utsunomiya, S. Goriely, T. Renstrøm, H.-T. Nyhus, O. Tesileanu, T. Glodariu, T. Shima, K. Takahisa, S. Miyamoto, Y.-W. Lui, S. Hilaire, S. Péru, M. Martini, and A. J. Koning, Phys. Rev. C **90**, 064616 (2014).
[26] H. Utsunomiya, S. Katayama, I. Gheorghe, S. Imai, H. Yamaguchi, D. Kahl, Y. Sakaguchi, T. Shima, K. Takahisa, and S. Miyamoto, Phys. Rev. C **92**, 064323 (2015).
[27] T. Kondo, H. Utsunomiya, H. Akimune, T. Yama-gata, A. Okamoto, H. Harada, F. Kitatani, T. Shima, K. Horikawa, and S. Miyamoto, Nucl. Instrum. Methods Phys. Res. A **659**, 462 (2011).
[28] H. Utsunomiya, T. Watanabe, T. Ari-izumi, D. Takenaka, T. Araki, K. Tsuji, I. Gheorghe, D. M. Filipescu, S. Belyshev, K. Stopani, D. Symochko, H. Wang, G. Fan, T. Renstrøm, G. M. Tveten, Y.-W. Lui, K. Sugita, and S. Miyamoto, Nucl. Instrum. Methods Phys. Res. A **896**, 103 (2018).
[29] O. Itoh, H. Utsunomiya, H. Akimune, T. Kondo, M. Kamata, T. Yamagata, H. Toyokawa, H. Harada, F. Kitatani, S. Goko, C. Nair, and Y.-W. Lui, J. Nucl. Sci. Technol **48**, 834 (2011).
[30] J. Allison *et al.*, IEEE T. Nucl. Sci. **53**, 270 (2006).
[31] T. Renstrøm, H. Utsunomiya, H. T. Nyhus, A. C. Larsen, M. Guttormsen, G. M. Tveten, D. M. Filipescu, I. Gheorghe, S. Goriely, S. Hilaire, Y.-W. Lui, J. E. Midtbø, S. Péru, T. Shima, S. Siem, and O. Tesileanu, Phys. Rev. C **98**, 054310 (2018).
[32] A. P. Tonchev, S. L. Hammond, J. H. Kelley, E. Kwan, H. Lenske, G. Rusev, W. Tornow, and N. Tsoneva, Phys. Rev. Lett. **104**, 072501 (2010).
[33] S. Goriely, P. Dimitriou, M. Wiedeking *et al.*, Eur. Phys. J. A (to be published).
[34] B. L. Berman, S. C. Fultz, J. T. Caldwell, M. A. Kelly, and S. S. Dietrich, Phys. Rev. C **2**, 2318 (1970).
[35] V. V. Varlamov, B. S. Ishkhanov, V. N. Orlin, and N. N. Peskov, Yad. Fiz. **79**, 315 (2016).
[36] A. J. Koning, S. Hilaire, and S. Goriely, Nucl. Phys. A **810**, 13 (2008).
[37] S. Goriely, S. Hilaire, and A. J. Koning, Phys. Rev. C **78**, 064307 (2008).
[38] D. B. Stroud and D. M. H. Chan, Astrophys. J. **178**, L93 (1972).
[39] F. Voss, K. Wisshak, and F. Kappeler, Phys. Rev. C **52**, 1102 (1995).
[40] F. Voss, K. Wisshak, K. Guber, F. Kappeler, and G. Reffo, Phys. Rev. C **50**, 2582 (1994).
[41] P. E. Koehler, R. R. Spencer, K. H. Guber, R. R. Winters, S. Raman, J. A. Harvey, N. W. Hill, J. C. Blackmon, D. W. Bardayan, D. C. Larson, T. A. Lewis, D. E. Pierce, and M. S. Smith, Phys. Rev. C **57**, R1558 (1998).
[42] A. R. DeL. Musgrove, B. J. Allen, J. W. Baldeman, and R. L. Macklin, Int. Conf. Neutr. Phys. Nucl. Data, Harwell (1978), p. 449.
[43] Z. Y. Bao, H. Beer, F. Käppeler, F. Voss, K. Wisshak, and T. Rauscher, At. Data Nucl. Data Tables **75**, 1 (2000).